Suppression of Interband Heating for Random Driving

Hongzheng Zhao,[1,2] Johannes Knolle,[3,4,2] Roderich Moessner,[1] and Florian Mintert[2,5]
[1]Max-Planck-Institut für Physik komplexer Systeme, Nöthnitzer Straße 38, 01187 Dresden, Germany
[2]Blackett Laboratory, Imperial College London, London SW7 2AZ, United Kingdom
[3]Department of Physics TQM, Technische Universität München, James-Franck-Straße 1, D-85748 Garching, Germany
[4]Munich Center for Quantum Science and Technology (MCQST), 80799 Munich, Germany
[5]Helmholtz-Zentrum Dresden-Rossendorf, Bautzner Landstraße 400, 01328 Dresden, Germany

(Received 20 January 2022; revised 22 March 2022; accepted 31 August 2022; published 14 September 2022)

Heating to high-lying states strongly limits the experimental observation of driving induced nonequilibrium phenomena, particularly when the drive has a broad spectrum. Here we show that, for entire families of structured random drives known as random multipolar drives, particle excitation to higher bands can be well controlled even away from a high-frequency driving regime. This opens a window for observing drive-induced phenomena in a long-lived prethermal regime in the lowest band.

DOI: 10.1103/PhysRevLett.129.120605

Introduction.—Quantum simulators hold the promise of exploring physics that is far beyond the capabilities of any conceivable classical simulation. A crucial tool is driving quantum systems, since this can result in drastic modifications of their properties [1–7]. Particularly, periodic driving is used to *Floquet engineer* either time-independent effective models with exotic physical processes [8,9] and time-dependent models exhibiting nonequilibrium phases of matter which do not exist in static systems [10]. Prominent examples include Floquet time crystals [11,12], artificial gauge fields for neutral particles [13–15], novel topological phases of matter [16–18].

Actual limitations of successful Floquet engineering result from heating [19–22]: in addition to the desired modification of quantum dynamics, driving also induces undesired transitions to excited states. In the case of lattice models with a well-defined band structure, the heating effects can be categorized into two classes. Excitation to higher bands (interband heating) inevitably leads to particle loss from the lowest band that is typically used for the quantum simulation [21,23]; and even if interband heating is sufficiently slow, intraband heating lets any generic many-body system thermalize to a high-temperature state within the lowest band [24–26].

Quantum simulations thus typically rely on the existence of a sweet spot of drives that can induce the desired dynamics without causing too much heating. Periodic driving allows to suppress intraband heating in terms of a sufficiently high fundamental frequency [27–31]. Many-body resonances in the low-energy subspace are exponentially suppressed, so that a quasistationary prethermal regime can exist. Within the lowest-band approximation, the lifetime of the prethermal regime can be arbitrarily long for a sufficiently fast drive. In realistic many-band systems, however, the transitions to higher bands that can become resonant with high-frequency driving pose severe limitations to the practically accessible driving spectra [32]. Due to the discrete spectrum of periodic driving, this is not an unsurmountable obstacle, and there are driving frequencies that give access to long-lived Floquet prethermalization in a series of quantum systems, including NV centers [33], trapped ions [34], NMR [35] and Hubbard type systems [19,21].

Aperiodic driving can generate novel nonequilibrium phases beyond the Floquet paradigm [36–42] and achieve better performance on programmable quantum processors [43–46]. However, quantum simulations are still mostly based on periodic protocols because the broader spectra of aperiodic drives make it much more challenging to find driving patterns that realize desired dynamics without excessive heating. Prethermalization can occur also for quasiperiodic [47,48] and structured random drives [40], but interband heating with aperiodic driving is a largely uncharted territory. The complicated spectrum can potentially induce stronger particle loss than with periodic drives, and the existence of a long-lived prethermal regime is not guaranteed.

In this work, we show that random multipolar driving (RMD) [40,48], which interpolates between random and quasiperiodic drives, can still provide access to long-lived prethermal phenomena. We focus on the basic Bose-Hubbard model (BHM) which is standardly realized in current experiments with ultracold atoms trapped in optical

lattices. We discover a highly nonmonotonic dependence of the interband heating on the driving frequency. Most importantly, within specific frequency windows, interband heating can be exceptionally suppressed, when a single particle can approximately complete Rabi-like cycles between the bands and recover its initial state at stroboscopic times. Since this suppression extends to situations where many-body interactions are present as long as the band gap is sufficiently large, our findings can directly be tested in current experiments [19,21]. It also provides a sufficiently long time interval to observable long-lived prethermalization in the lowest band within suitable frequency windows.

The model.—The dynamics of spinless bosons within a single band is characterized by the Hamiltonian

$$\hat{H}(J,U,\vec{h},\vec{b}) = -J\sum_l(\hat{b}_{l+1}^\dagger\hat{b}_l + \text{H.c.}) + \frac{U}{2}\sum_l \hat{n}_l(\hat{n}_l-1) + \sum_l h_l\hat{n}_l, \quad (1)$$

with hopping rate J, interaction constant U, onsite energies h_l and bosonic creation operators $\hat{b}_l^\dagger$, and number operators $\hat{n}_l = \hat{b}_l^\dagger\hat{b}_l$ on sites labeled by l in the corresponding band.

The low-energy subspace is the s band with Hamiltonian $\hat{H}_s = \hat{H}(J_s,U_s,\vec{h},\vec{b}_s)$. Since the hopping rate can be directly tuned via the lattice depth, it is common to realize a time-dependent Hamiltonian in terms of a time-dependent hopping rate. In the following, we thus consider the piecewise constant drive of the s-band BHM $\hat{H}_{s,\pm} = \hat{H}(J_s \pm \delta J_s, U_s, \vec{h}, \vec{b}_s)$ for the n-RMD protocol specified later.

Modulation of the lattice depth excites particles to higher bands. As the first excited (p) band has odd parity, transitions from the even-parity s band to higher bands are dominated by the coupling to the second excited (d) band [19]. Higher bands beyond the d band do exist but they are less relevant for our purpose in a sufficiently deep lattice [23]. Including the d band in terms of the Hamiltonian $\hat{H}_d = \hat{H}(J_d,U_d,\vec{h}+\Delta,\vec{b}_d)$ with an energy gap Δ to the s band is the central step in going beyond the lowest-band-approximation. This energy gap is normally much larger than the s-band hopping rate J_s; in a deep lattice it can even be larger by 2 orders of magnitude [19,21,32]. The Hamiltonian [7,21,32]

$$\hat{H}_{sd} = U_{sd}\sum_l\left[2\hat{n}_{sl}\hat{n}_{dl} + \frac{1}{2}(\hat{b}_{dl}^\dagger\hat{b}_{dl}^\dagger\hat{b}_{sl}\hat{b}_{sl} + \text{H.c.})\right], \quad (2)$$

where the index sl or dl labels site l in the s or d band, respectively, captures the interband interaction including an on-site density-density interaction and simultaneous hopping of two particles between the bands. Modulation of the lattice depth changes not only the hopping rate in the s band, but it also induces single particle interband transitions to the d band [21,32] as described by the Hamiltonian

$$\hat{H}_{\text{tr}} = \eta\delta J_s\sum_l \hat{b}_{dl}^\dagger\hat{b}_{sl} + \text{H.c.}, \quad (3)$$

with a dimensionless transition ratio η. Strictly speaking the lattice modulation will also let parameters like the hopping rate in the d band or the interaction amplitudes vary in time. However, this time dependency will not lead to sizable effects as long as the band gap is sufficiently large. Therefore, in addition to the s-band drive, we only consider the driving dependent single particle transitions.

Our goal is to investigate the heating process of the two-band BHM subject to the RMD protocol [40], which can be defined as a sequence of the two piecewise constant Hamiltonians $\hat{H}_\pm = \hat{H}_{s,\pm} + \hat{H}_d + \hat{H}_{sd} \pm \hat{H}_{\text{tr}}$. A period of deterministic dynamics over a time window of length 2^nT can be defined recursively via the time evolution operators $U_n^\pm = U_{n-1}^\mp U_{n-1}^\pm$, with $U_0^\pm = e^{-iT\hat{H}_\pm}$. Temporal randomness can be introduced by concatenating dynamics over several such time windows with the operator $U_n^\pm$ chosen at random. Extra time dependence in the protocol is permitted within each time window T to engineer novel micromotions [48,49] or to implement trotterization for digital quantum simulations [43].

Long-lived prethermalization governed by the effective Hamiltonian $\hat{H}_{\text{eff}} = \hat{H}_+ + \hat{H}_-$ is predicted [40,48] in the rapid driving regime where the characteristic driving frequency $1/T$ is the dominant energy scale. The scaling $\tau_{\text{pre}} \sim T^{-(2n+1)}$ of the prethermal lifetime has been observed numerically in nonintegrable spin models [40,48], in contrast to the exponential scaling observed in Floquet systems [19,50]. In the following, we first establish similar prethermal phenomena in the lowest s band. Taking into account multiple bands, we then confirm the characteristic scaling of the prethermal lifetime even though $1/T$ is only larger than the energy scales of the lower band but smaller than the gap to higher ones.

Prethermalization in the s band.—The existence of a prethermal regime within the lowest-band approximation is indicated in Fig. 1 with dynamics following an average over 100 instances of 2-RMD driving with periodic boundary conditions. The initial state is chosen as a density-wave state in the lattice of $L = 12$ sites and total particle number $N_{\text{tot}} = 6$. Onsite energies $\vec{h}$ are chosen as $-\mu$ on even sites and 0 on odd sites. Such a potential difference enables the system to maintain the density-wave configuration in the prethermal regime.

Inset (a) depicts the normalized energy $\varepsilon(t) \equiv (E_t - E_0)/(E_\infty - E_0)$, with the energy expectation $E_t = \langle\Psi_t|\hat{H}_{\text{eff}}|\Psi_t\rangle$ taken with respect to the effective Hamiltonian, the infinite temperature energy $E_\infty = \text{Tr}\hat{H}_{\text{eff}}/D$, where D is the Hilbert

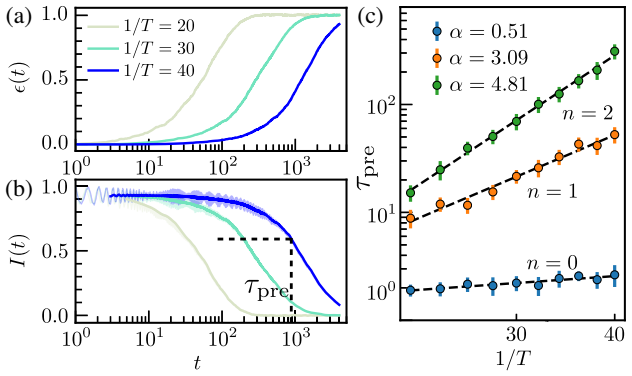

FIG. 1. Dynamics of the energy (a) and imbalance (b) for the s-band BHM. A prethermal plateau appears in both panels with a lifetime $\tau_{\rm pre}$ increasing with driving frequency $1/T$. (c) Algebraic scaling $\tau_{\rm pre} \sim T^{-(2n+1)}$ can be observed for $n \geq 1$, whereas for $n = 0$, heating rapidly happens ($t \sim 1$). The follow parameters are used for numerical simulation $J_s = 1, \delta J_s = 0.9, U_s = 5, \mu = 10$.

space dimension and the energy $E_0 = \langle \Psi_0 | \hat{H}_{\rm eff} | \Psi_0 \rangle$ of the initial state $|\Psi_0\rangle$. Inset (b) shows the imbalance between the occupation on even and odd sites labeled by sl in the s band $I(t) = (2/L)(\sum_{l,\rm even} \langle \hat{n}_{sl} \rangle_t - \sum_{l,\rm odd} \langle \hat{n}_{sl} \rangle_t)$, with the occupation number expectation value $\langle \hat{n}_{sl} \rangle_t = \langle \Psi_t | \hat{n}_{sl} | \Psi_t \rangle$.

For the three representative values of the driving frequency $1/T$ shown in Figs. 1(a) and 1(b), the values of ε and I remain approximately constant during the prethermal plateau. Eventually they approach their infinite temperature value on some finite timescale, which depends on $1/T$, with fast driving (large values of $1/T$) favoring slow thermalization. The transition between the initial and final values of ε at any given value of $1/T$ takes place in the same time window as the corresponding transition of I, indicating that the definition of the prethermal lifetime $\tau_{\rm pre}$ is largely independent of the choice of observable whose thermalization is being characterized.

Defining the time t_x via $I(t_x) = x$, we extract the prethermal lifetime as the average $\tau_{\rm pre} = \langle t_x \rangle_x$, where the average over the five values $x = 0.8, 0.8 \pm 0.015$ and 0.8 ± 0.03 is performed to reduce numerical noise. Figure 1(c) depicts the dependence of $\tau_{\rm pre}$ on $1/T$ for different multipolar orders $n = 0$, 1, and 2. For $n = 1$ and 2, the numerical results are consistent with the predicted scaling law $\tau_{\rm pre} \sim T^{-(2n+1)}$ [40]. For the purely random drive $n = 0$, however, heating is always fast with only a weak dependence on the driving frequency, suggesting that the multipolar structure provides a qualitative improvement for controlling the intraband heating [40].

Apart from the case of purely random driving, n RMD of the single-band model thus allows us to increase the prethermal lifetime by choosing a sufficiently large driving frequency $1/T$. The existence of higher bands in real systems, however, imposes limitations to these choices because fast driving can result in interband heating.

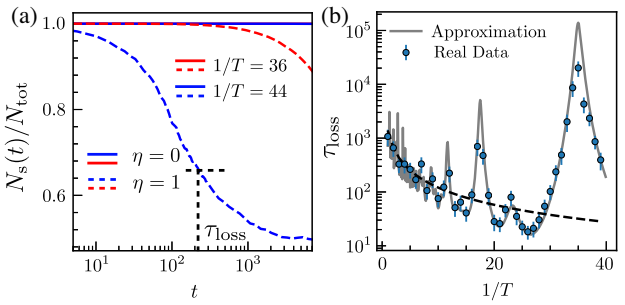

FIG. 2. (a) Dynamics of the relative population in s band for the 2 RMD. Solid or dashed lines correspond to zero or finite single particle excitations to the d band, respectively. Particle loss has a strong dependence on the driving frequency for $\eta = 1$. (b) Dependence of the particle loss timescale $\tau_{\rm loss}$ on the driving frequency $1/T$ for $\eta = 1$. Although in general larger $1/T$ induces more particle loss (the $t \sim T$ is depicted as a black dashed line to guide the eye), there exist several frequency windows where excitation to the d band is significantly suppressed. The parameters $\delta J_s = 1.2$, $J_d = 7$, $U_s = 5$, $U_d = 3$, $U_{sd} = 2$, $\mu = 10$, $\Delta = 220$ are used for numerical simulation.

Particle excitation to higher bands.—Both the collective hopping [Eq. (2)] and the single particle transitions [Eq. (3)] can result in particle excitations to the d band, and comparison between dynamics with $\eta = 0$ and with $\eta = 1$ helps to distinguish between these two processes. Figure 2(a) depicts 2-RMD dynamics of the relative population $N_s/N_{\rm tot}$ of particles number in the s band. The initial state is chosen as a density-wave state in the s band with total particle number $N_{\rm tot} = 4$ and $L = 8$ sites. Solid lines correspond to a system without single-particle interband transitions ($\eta = 0$), whereas dashed lines correspond to the case with a finite transition ratio $\eta = 1$. Red and blue colors indicate the two driving frequencies $1/T = 36$ and 44. For $\eta = 0$ (solid), the relative population remains practically constant for both driving frequencies. It thus suggests that although the interband interaction U_{sd} is nonzero, collective hopping events are rare due to the low filling factor. In contrast, finite single-particle transitions (dashed) result in notable particle loss to the d band, highlighting that this process dominates the interband heating.

It is worth noting that the interband heating exhibits a strong dependence on the driving frequency: In the case of the faster of the two drives (blue), the asymptotic equal distribution of particles over both bands is reached around $t \sim 10^3$, but for the slower drive (red), at the same time, the population remains almost fully in the s band.

The particle loss time $\tau_{\rm loss}$ at which the relative population $N_s/N_{\rm tot}$ falls below the threshold value of 0.92 [51] is depicted versus the frequency $1/T$ with blue dots in Fig. 2(b). Crucially, the dependence is highly nonmonotonic with a series of well-pronounced peaks that indicate frequency regimes in which heating to the d band is strongly suppressed. In the relatively slow driving regime

$(1/T < 10)$ the loss time follows the proportionality $\tau_{\text{loss}} \sim T$ (black dashed line), confirming that faster driving yields stronger interband heating [32]. While for faster driving $(1/T > 10)$, the particle loss time τ_{loss} oscillates around this proportionality, the amplitude of the oscillations are extremely large. For example, in the frequency window $30 < 1/T < 40$ the actual values of τ_{loss} can exceed the proportionality relation by more than 2 orders of magnitude.

Tractable model for the heating profile.—As the interband heating is strongly dominated by single-particle processes, we can provide an analytic approximation to the heating profiles shown in Fig. 2(b). Neglecting interactions and performing an average over the random choices of time evolution operators in the n-RMD protocol yields an exactly solvable model. Although it is not necessary for solvability, one may further neglect the modulation in the s-band hopping and the staggered potential, as they mainly affect the s-band prethermal dynamics but not the interband heating as long as the band gap is sufficiently large, see Supplemental Material [52].

Within this approximation, the two-band Hamiltonian can be expressed as $\hat{H}_{\pm} = \sum_k \hat{\boldsymbol{b}}_k^{\dagger} \hat{H}_k^{\pm} \hat{\boldsymbol{b}}_k$ with the matrix

$$\hat{H}_k^{\pm} = \begin{pmatrix} -2J_s \cos(k) & \pm\delta J_s \eta \\ \pm\delta J_s \eta & -2J_d \cos(k) + \Delta \end{pmatrix}, \tag{4}$$

and the vector $\hat{\boldsymbol{b}}_k^{\dagger} = (\hat{b}_{sk}^{\dagger}, \hat{b}_{dk}^{\dagger})$ of the creation operator in quasimomentum space. The dynamics decomposes into independent quasimomentum components, and the elementary time evolution operator in any given component reads $U_0^{\pm}(k) = [C_{0,0}\mathbf{1} + i(\pm C_{0,1}\hat{\sigma}_x + C_{0,2}\hat{\sigma}_z)]e^{i\phi_0}$, with k-dependent complex scalars $C_{0,j}$, phases ϕ_0, the Pauli matrices $\hat{\sigma}_{x,y,z}$, and the identity $\mathbf{1}$. The resulting multipolar operator of nth order reads $U_n^{\pm}(k) = [C_{n,0}\mathbf{1} + i(\pm C_{n,1}\hat{\sigma}_{[n]} + C_{n,2}\hat{\sigma}_z)]e^{i\phi_n}$, where $[n] = x$ for even n and $[n] = y$ for odd n, and the k-dependent coefficients $C_{n,j}$ are determined by the recursive relations

$$C_{n+1,0} = -2C_{n,2}^2 + 1, \qquad C_{n+1,2} = 2C_{n,2}C_{n,0},$$
$$C_{n+1,1} = -2C_{n,2}C_{n,1}\varepsilon_{z,[n],[n+1]}, \tag{5}$$

where $\varepsilon_{z,[n],[n+1]}$ denotes the Levi-Civita symbol, see Supplemental Material [52].

The time evolution of a single-particle quasimomentum eigenstate $|\psi_k\rangle = \hat{b}_{sk}^{\dagger}|0\rangle$ is particularly simple but enlightening when $C_{n,1}(k)$ vanishes. This particle oscillates between the two bands, however, as $U_n^{\pm}(k)$ is now diagonal, it completes a full Rabi cycle at the end of each time window of length $2^n T$. Although different hopping processes between the two bands are permitted, they can interfere destructively [53–55] to keep the initial state localized in the s band, hence, no particle loss happens at stroboscopic times. The dynamics averaged over random choices of the n-RMD protocol is still exactly solvable even if we deviate from this special case. To do so, we use the density matrix ϱ_k^m to represent the state for the k component at time $t = 2^n T m$ after the temporal random average [56]. The time evolution can thus be obtained recursively as $\varrho_k^{m+1} = \frac{1}{2}U_n^{+}\varrho_k^m(U_n^{+})^{\dagger} + \frac{1}{2}U_n^{-}\varrho_k^m(U_n^{-})^{\dagger}$ with the initial state $\varrho_k^0 = |\psi_k\rangle\langle\psi_k|$. The resulting density matrix at later times reads $\varrho_k^m = f_m\varrho_k^0 + g_m\mathbf{1}$ with coefficients f_m and g_m exactly solvable by induction (see Supplemental Material [52]).

Even though the dynamics itself does not lead to mixing of different quasimomenta in the density matrix, generic initial states may have such components. These, however, average out, and the systems' dynamics can be well approximated by the incoherent sum over all momenta. If we initialize a Fock state in the s band, the particle can still complete Rabi-like cycles between two bands at stroboscopic times if the difference between the intraband hopping rates is much smaller than the band gap $(J_d - J_s \ll \Delta)$, see Supplemental Material [52]. The resulting population in the s band is then approximated as $N_s(2^n Tm) \simeq 1/2 + \sum_k (1 - 2C_{n,1}^2)^m/2L$, suggesting that the population in the s band decreases exponentially in time. The particle loss time τ_{loss} derived from this model is depicted as a gray line in Fig. 2(b), which coincides very accurately with the exact numerical data [57].

Protection of prethermalization.—Particle loss to higher bands generally prevents the observation of prethermalization in the lowest band. However, the ability to predict regimes of slow interband heating can be used to identify suitable prethermalization regimes. With the driving frequency $1/T = 36$, for example, τ_{loss} is around 10^4 [as shown in Fig. 2(b)] which is sufficiently long to make it irrelevant for the prethermal dynamics. Therefore, as shown in Fig. 3(a), there is hardly any noticeable difference between the dynamics with $\eta = 0$ (solid) and with $\eta = 1$ (dashed) for the red data. But for $1/T = 44$ (blue) for which $\tau_{\text{loss}} \sim 10^2$ is comparable to the prethermal timescale, heating within the s band is significantly accelerated by single-particle interband transitions.

The prethermal lifetime τ_{pre} defined in terms of the threshold value 0.55 [58] for the imbalance I in the presence of single particle transition $(\eta = 1)$ is depicted as a function of the driving frequency $1/T$ in Fig. 3(b) on a log-log scale. Apart from the regime of extremely fast driving, as well as the region $25 \lesssim 1/T \lesssim 30$, the numerical data agree well with the algebraic scaling $\tau_{\text{pre}} \sim T^{-(2n+1)}$ with $n = 2$ indicated by a dashed line. In particular, in the regime $31 \lesssim 1/T \lesssim 39$, the prethermal lifetime in the range $100 \lesssim \tau_{\text{pre}} \lesssim 400$ is substantially shorter than the particle loss time (gray line). Modulation of interactions in general accelerates the interband heating, but it only causes negligible effects to the prethermal lifetime, see Supplemental Material [52].

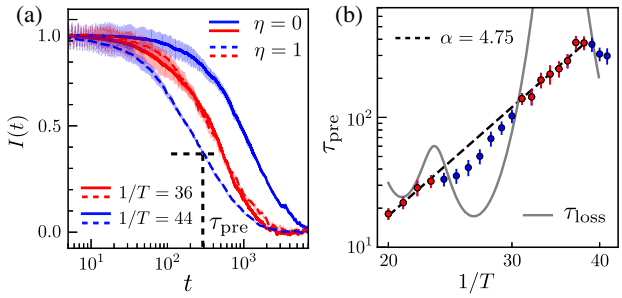

FIG. 3. (a) Dynamics of the imbalance in the s band for 2 RMD. For $1/T = 44$, the imbalance rapidly decays to zero, whereas for $1/T = 36$, the prethermalization remains almost unchanged as notable particle loss only occurs at a later timescale. (b) When particle loss occurs slowly (red dots), the prethermal lifetime $\tau_{\rm pre}$ fits well to an algebraic scaling with exponent $\alpha \approx 2n + 1$. Otherwise, the s band thermalizes faster (blue dots).

Discussion.—The nonmonotonic suppression of interband heating and the long-lived prethermal regime in RMD systems can be detected via existing experimental techniques. For instance, with cold atoms trapped in optical lattices, the required initial density-wave state can be prepared [6,59] and the band gap is tunable from $40J_s$ to $500J_s$ [19]. Additionally, the accessible coherent lifetime is longer than the prethermal lifetime $\tau_{\rm pre}$ [19,59,60], and the occupation imbalance $I(t)$ in the s band can be measured via fluorescence imaging [1,19]. Once the long-lived prethermalization is established, it would be intriguing to engineer prethermal phases of matter with novel correlations in the micromotions unobtainable with periodic drives. Also, using suitable choices of the elementary unitaries $U_0^{\pm}$ in the RMD sequence can form the basis of quantum simulations beyond the paradigm of Floquet engineering.

The observation that single-particle interband tunneling is the leading cause of interband heating for random drives is one of the key findings of this work. It allows us to derive an analytically tractable and intuitive model which accurately captures the nonmonotonic heating profile. This heating profile is largely independent of the underlying Hamiltonian as long as there is a large gap between the bands. Also, it does not require the driving frequency to be the dominant energy scale as in previous works based on a high frequency expansion [48]. Therefore, our work provides a new setting for probing the slow thermalization phenomena. It remains intriguing to investigate whether the exact solution of the RMD two-level systems can be applied to other contexts, e.g., for integrable many-body systems. It will also be interesting to explore interband heating effects for dynamical localization [54,61] or the stability of quantum many-body scars [62–65].

In higher dimensions, lattice geometry plays an important role in suppressing interband heating for periodic drives [60]. It will thus be interesting to explore geometric effects on n-RMD drives, the role of dimensionality or the particle density dependence. Reliable numerical simulations of higher dimensional systems normally lie beyond the capability of classical methods especially for random drives. Therefore, experimental investigation of the interband heating in quantum simulators would be highly welcome.

We acknowledge very helpful discussions with Monika Aidelsburger and for bringing the importance of interband heating to our attention. We are also grateful for discussions with Bing Yang, Joseph Vovrosh, and Frédéric Sauvage. H. Z. acknowledges support from a Doctoral-Program Fellowship of the German Academic Exchange Service (DAAD). We acknowledge support from the Imperial-TUM flagship partnership. This work was partly supported by the Deutsche Forschungsgemeinschaft under grants SFB 1143 (project-id 247310070) and the cluster of excellence ct.qmat (EXC 2147, project-id 390858490). The research is part of the Munich Quantum Valley, which is supported by the Bavarian state government with funds from the Hightech Agenda Bayern Plus.

[1] J. F. Sherson, C. Weitenberg, M. Endres, M. Cheneau, I. Bloch, and S. Kuhr, Nature (London) **467**, 68 (2010).
[2] E. A. Martinez, C. A. Muschik, P. Schindler, D. Nigg, A. Erhard, M. Heyl, P. Hauke, M. Dalmonte, T. Monz, P. Zoller *et al.*, Nature (London) **534**, 516 (2016).
[3] R. Moessner and S. L. Sondhi, Nat. Phys. **13**, 424 (2017).
[4] F. Arute, K. Arya, R. Babbush, D. Bacon, J. C. Bardin, R. Barends, R. Biswas, S. Boixo, F. G. Brandao, D. A. Buell *et al.*, Nature (London) **574**, 505 (2019).
[5] K. Wintersperger, C. Braun, F. N. Ünal, A. Eckardt, M. Di Liberto, N. Goldman, I. Bloch, and M. Aidelsburger, Nat. Phys. **16**, 1058 (2020).
[6] B. Yang, H. Sun, R. Ott, H.-Y. Wang, T. V. Zache, J. C. Halimeh, Z.-S. Yuan, P. Hauke, and J.-W. Pan, Nature (London) **587**, 392 (2020).
[7] B. Song, S. Dutta, S. Bhave, J.-C. Yu, E. Carter, N. Cooper, and U. Schneider, Nat. Phys. **18**, 259 (2022).
[8] T. Oka and S. Kitamura, Annu. Rev. Condens. Matter Phys. **10**, 387 (2019).
[9] M. Bukov, L. D'Alessio, and A. Polkovnikov, Adv. Phys. **64**, 139 (2015).
[10] A. Eckardt, Rev. Mod. Phys. **89**, 011004 (2017).
[11] V. Khemani, A. Lazarides, R. Moessner, and S. L. Sondhi, Phys. Rev. Lett. **116**, 250401 (2016).
[12] D. V. Else, B. Bauer, and C. Nayak, Phys. Rev. Lett. **117**, 090402 (2016).
[13] J. Struck, M. Weinberg, C. Ölschläger, P. Windpassinger, J. Simonet, K. Sengstock, R. Höppner, P. Hauke, A. Eckardt, M. Lewenstein *et al.*, Nat. Phys. **9**, 738 (2013).
[14] M. Aidelsburger, M. Atala, M. Lohse, J. T. Barreiro, B. Paredes, and I. Bloch, Phys. Rev. Lett. **111**, 185301 (2013).
[15] C. Gross and I. Bloch, Science **357**, 995 (2017).
[16] F. Nathan, D. Abanin, E. Berg, N. H. Lindner, and M. S. Rudner, Phys. Rev. B **99**, 195133 (2019).

[17] F. Nathan, M. S. Rudner, N. H. Lindner, E. Berg, and G. Refael, Phys. Rev. Lett. **119**, 186801 (2017).
[18] T. Kitagawa, E. Berg, M. Rudner, and E. Demler, Phys. Rev. B **82**, 235114 (2010).
[19] A. Rubio-Abadal, M. Ippoliti, S. Hollerith, D. Wei, J. Rui, S. L. Sondhi, V. Khemani, C. Gross, and I. Bloch, Phys. Rev. X **10**, 021044 (2020).
[20] M. Reitter, J. Näger, K. Wintersperger, C. Sträter, I. Bloch, A. Eckardt, and U. Schneider, Phys. Rev. Lett. **119**, 200402 (2017).
[21] K. Viebahn, J. Minguzzi, K. Sandholzer, A.-S. Walter, M. Sajnani, F. Görg, and T. Esslinger, Phys. Rev. X **11**, 011057 (2021).
[22] K. Sandholzer, A.-S. Walter, J. Minguzzi, Z. Zhu, K. Viebahn, and T. Esslinger, Phys. Rev. Research **4**, 013056 (2022).
[23] C. Sträter and A. Eckardt, Z. Naturforsch. A **71**, 909 (2016).
[24] A. Lazarides, A. Das, and R. Moessner, Phys. Rev. E **90**, 012110 (2014).
[25] D. A. Abanin, W. De Roeck, and F. Huveneers, Phys. Rev. Lett. **115**, 256803 (2015).
[26] T. Mori, T. N. Ikeda, E. Kaminishi, and M. Ueda, J. Phys. B **51**, 112001 (2018).
[27] T. Kuwahara, T. Mori, and K. Saito, Ann. Phys. (Amsterdam) **367**, 96 (2016).
[28] D. Abanin, W. De Roeck, W. W. Ho, and F. Huveneers, Commun. Math. Phys. **354**, 809 (2017).
[29] A. Eckardt and E. Anisimovas, New J. Phys. **17**, 093039 (2015).
[30] F. Machado, D. V. Else, G. D. Kahanamoku-Meyer, C. Nayak, and N. Y. Yao, Phys. Rev. X **10**, 011043 (2020).
[31] A. Pizzi, A. Nunnenkamp, and J. Knolle, Phys. Rev. Lett. **127**, 140602 (2021).
[32] G. Sun and A. Eckardt, Phys. Rev. Research **2**, 013241 (2020).
[33] W. Beatrez, O. Janes, A. Akkiraju, A. Pillai, A. Oddo, P. Reshetikhin, E. Druga, M. McAllister, M. Elo, B. Gilbert *et al.*, Phys. Rev. Lett. **127**, 170603 (2021).
[34] A. Kyprianidis, F. Machado, W. Morong, P. Becker, K. S. Collins, D. V. Else, L. Feng, P. W. Hess, C. Nayak, G. Pagano *et al.*, Science **372**, 1192 (2021).
[35] P. Peng, C. Yin, X. Huang, C. Ramanathan, and P. Cappellaro, Nat. Phys. **17**, 444 (2021).
[36] A. Verdeny, J. Puig, and F. Mintert, Z. Naturforsch. A **71**, 897 (2016).
[37] S. Nandy, A. Sen, and D. Sen, Phys. Rev. X **7**, 031034 (2017).
[38] P. T. Dumitrescu, R. Vasseur, and A. C. Potter, Phys. Rev. Lett. **120**, 070602 (2018).
[39] H. Zhao, F. Mintert, and J. Knolle, Phys. Rev. B **100**, 134302 (2019).
[40] H. Zhao, F. Mintert, R. Moessner, and J. Knolle, Phys. Rev. Lett. **126**, 040601 (2021).
[41] S. Choudhury and W. V. Liu, arXiv:2109.05318.
[42] G. Guarnieri, M. T. Mitchison, A. Purkayastha, D. Jaksch, B. Buča, and J. Goold, arXiv:2104.13402.
[43] M. Heyl, P. Hauke, and P. Zoller, Sci. Adv. **5**, eaau8342 (2019).
[44] A. M. Childs, A. Ostrander, and Y. Su, Quantum **3**, 182 (2019).
[45] H. R. Grimsley, D. Claudino, S. E. Economou, E. Barnes, and N. J. Mayhall, J. Chem. Theory Comput. **16**, 1 (2019).
[46] P. T. Dumitrescu, J. Bohnet, J. Gaebler, A. Hankin, D. Hayes, A. Kumar, B. Neyenhuis, R. Vasseur, and A. C. Potter, Nature (London) **607**, 463 (2022).
[47] D. V. Else, W. W. Ho, and P. T. Dumitrescu, Phys. Rev. X **10**, 021032 (2020).
[48] T. Mori, H. Zhao, F. Mintert, J. Knolle, and R. Moessner, Phys. Rev. Lett. **127**, 050602 (2021).
[49] H. Zhao, M. S. Rudner, R. Moessner, and J. Knolle, Phys. Rev. B **105**, 245119 (2022).
[50] F. Machado, G. D. Kahanamoku-Meyer, D. V. Else, C. Nayak, and N. Y. Yao, Phys. Rev. Research **1**, 033202 (2019).
[51] Similarly to above, numerical noise can be suppressed in terms of an average over the threshold values 0.92, 0.92 ± 0.015, and 0.92 ± 0.03.
[52] See Supplemental Material at http://link.aps.org/supplemental/10.1103/PhysRevLett.129.120605 for details of the analytical estimation of the interband heating and numerical data for interband heating dependence on the band gap and interaction modulation.
[53] F. Grossmann, T. Dittrich, P. Jung, and P. Hänggi, Phys. Rev. Lett. **67**, 516 (1991).
[54] A. Das, Phys. Rev. B **82**, 172402 (2010).
[55] S. Mondal, D. Pekker, and K. Sengupta, Europhys. Lett. **100**, 60007 (2013).
[56] M. A. Nielsen and I. Chuang,Quantum Computation and Quantum Information: 10th Anniversary Edition (Cambridge University Press, 2012), 10.1017/CBO9780511976667.
[57] Even though the particle loss time is defined in terms of a threshold whose value can be chosen from a range of reasonable values, the agreement between analytic and numerical data cannot be attributed to a suitably chosen threshold value, since the particle loss time in both analytics and numerics is defined with respect to the same threshold value.
[58] Numerical noise can be suppressed in terms of an average over the threshold values 0.55, 0.55 ± 0.05, and 0.55 ± 0.025.
[59] S. Scherg, T. Kohlert, P. Sala, F. Pollmann, B. H. Madhusudhana, I. Bloch, and M. Aidelsburger, Nat. Commun. **12**, 4490 (2021).
[60] M. Messer, K. Sandholzer, F. Görg, J. Minguzzi, R. Desbuquois, and T. Esslinger, Phys. Rev. Lett. **121**, 233603 (2018).
[61] A. Haldar, D. Sen, R. Moessner, and A. Das, Phys. Rev. X **11**, 021008 (2021).
[62] C. J. Turner, A. A. Michailidis, D. A. Abanin, M. Serbyn, and Z. Papić, Nat. Phys. **14**, 745 (2018).
[63] B. Mukherjee, S. Nandy, A. Sen, D. Sen, and K. Sengupta, Phys. Rev. B **101**, 245107 (2020).
[64] H. Zhao, A. Smith, F. Mintert, and J. Knolle, Phys. Rev. Lett. **127**, 150601 (2021).
[65] M. Serbyn, D. A. Abanin, and Z. Papić, Nat. Phys. **17**, 675 (2021).